



COMPARISON OF TWO BI-PHASE HYBRID STEPPER MOTORS, ONE WITH A SOLID AND THE OTHER WITH A LAMINATED STATOR

TEODOR IONUȚ ICHIM¹, OVIDIU CRAIU¹

Keywords: Bi-phase hybrid stepper; Finite element method; Relative magnetic permeability of a laminated stack.

The authors modelled and compared two hybrid stepper motors (HSM) sharing identical geometrical characteristics, phase resistance, and supply voltage. One motor features a solid stator, while the other is equipped with a laminated stator. The paper details the implementation of a three-dimensional finite element method (FEM) model, which includes the calculation of the equivalent magnetic permeability in the direction perpendicular to the laminated stack. The solid motor produces higher torque than the laminated motor, making it a better choice for applications requiring high torque density at low speeds. Experimental results confirmed the findings from the numerical simulations. After calibrating the FEM model based on the numerical results, an optimisation of both motor versions was conducted.

1. INTRODUCTION

Calculating the static and cogging (or dented) torque characteristics of a Hybrid Stepper Motor (HSM) is challenging and requires three-dimensional numerical modeling. This difficulty arises from the motor's complex magnetic field distribution, which has transverse and axial components. As demonstrated in specialized literature, hybrid 2D Finite Element Method (FEM) models, when combined with analytically computed conditions such as additional boundary conditions, fail to yield accurate results [1,2]. In contrast, 3D models demand significant computational resources. Stueberg demonstrated in [3] that solving a single rotor position of an HSM in 2012 required over 29.5 hours when using a finite element mesh consisting of 3.2 million tetrahedra. Previous studies from the 1990s, such as [4], which claim to have conducted a three-dimensional numerical analysis to identify the optimal tooth geometry of an HSM, are difficult to accept due to the immense computational effort needed to achieve those results with the technology available at that time. Oswald also showed in his paper [5] that accurately determining the holding torque of an HSM was not feasible without employing a three-dimensional FEM model.

In addition, the special geometry of the HSM presents significant challenges for numerical computation. The high number of teeth on the stator and rotor, with their small dimensions and the narrow air gap, requires a refined discretisation mesh with a substantial number of finite elements.

Another complicating factor in the numerical modelling of HSM is its magnetic anisotropy. As Muller explained [6], the closure of the magnetic axial field is more difficult in the direction perpendicular to the lamination, as it travels through iron and insulation. The material inhomogeneity along the axial direction is reflected in an equivalent relative magnetic permeability much lower than the relative permeability in the transverse plane. This means that the motor exhibits strong anisotropic behaviour.

Consequently, the FEM Jacobian matrix becomes poorly conditioned, which adversely affects solution convergence. Therefore, the computation time required to model a magnetically anisotropic HSM with a laminated stator becomes significantly greater when compared to modelling a magnetically isotropic HSM, where both the rotor and stator are made of solid material.

This paper presents a 3D FEM model of a bi-phase HSM designed for space applications. The model calculates the

static and detent torque characteristics of the motor. In addition to the primary geometry of the HSM, the model considers the actual geometry of the end windings, magnetic leakage flux, and the fringing effect by incorporating an air envelope around the motor.

The analysis using the 3D FEM model shows that the size of the airgap and the stator stacking factor influence the motor's performance. Moreover, obtaining precise geometrical dimensions is technically challenging. For instance, the stator stacking factor for a specific lamination thickness is affected by the insulation layer between the sheets, which varies depending on the type of material used and the manufacturing technology employed [7].

Precise modelling and sizing of an HSM can be challenging, much like manufacturing the motor. This difficulty arises from the small air gap, which is characteristic of this type of motor and can be as narrow as 0.1 mm. Obtaining such dimensions requires high-precision manufacturing technologies.

Packing and gluing the stator laminations also poses challenges, particularly because stamped laminations require precise indexing. An alternative approach could be to cut the entire stack using Wire Electrical Discharge Machining (EDM), which offers high geometrical accuracy within microns while minimally impacting the magnetic properties of the laminations. In contrast, laser cutting tends to be less precise and generates high temperatures that could adversely affect the material's magnetic properties [8].

The results obtained with the FEM 3D model are very accurate, as demonstrated by the comparison between computed values and experimentally measured results presented at the end of the paper. The primary technological operations used to manufacture the motor, the test bench setup, and the test results are also discussed.

After calibrating the numerical model (by comparing results with experimental data), the HSM was geometrically optimised maintaining the motor's initial geometrical envelope, phase resistance, and supply voltage [9]. The new HSM produces a 30% increased holding torque, showing the importance of numerical modelling.

2. NUMERICAL MODEL

A 3D FEM model of the HSM was developed using the module *Rotating Machinery, Magnetic* of the professional software COMSOL Multiphysics. The module allows the combined utilisation of the formulations based on magnetic vector potential \mathbf{A} in the domains with electric currents:

¹ UNST Politehnica București, Facultatea de Inginerie Electrică, Splaiul Independenței nr. 313, sector 6, București, Romania.
E-mails: ichim_teorod@yahoo.com, ocraiu@yahoo.com

$$\nabla^2 \mathbf{A} = \Delta \mathbf{A} = -\mu \mathbf{J}_e, \quad (1)$$

with \mathbf{J}_e the current density in the element, and based on magnetic scalar potential V_m in domains without current sources:

$$\nabla \cdot (\mu(\mathbf{H}) \nabla V_m) = 0 \quad (2)$$

In the regions where permanent magnets are present the above relation becomes:

$$\nabla \cdot [\mu(\nabla V_m)] = \nabla \cdot \mathbf{B}_r, \quad (3)$$

which, considering the equivalent magnetic permeability μ constant in each finite element and the remanent magnetic flux density \mathbf{B}_r , becomes:

$$\Delta V_m = \frac{1}{\mu} \nabla \cdot \mathbf{B}_r. \quad (1)$$

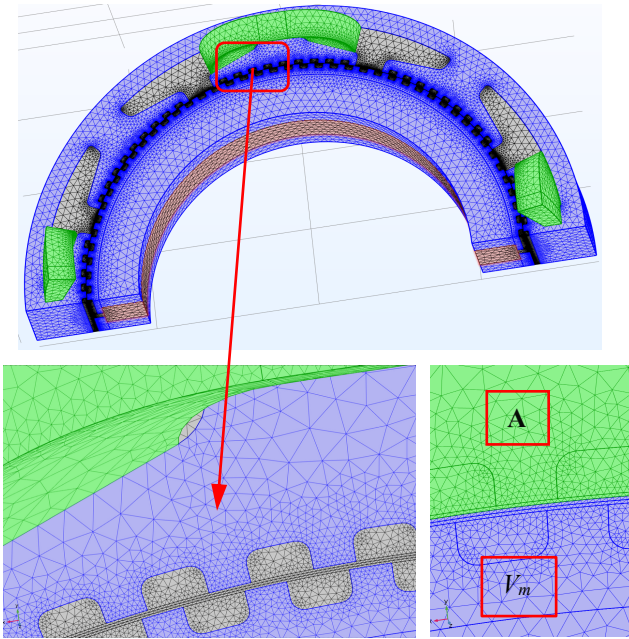


Fig. 1 – Discretization in elements of the studied domain: top – the ferromagnetic domain (blue), end windings (green), air (white) and permanent magnet (red), lower left – mesh detail at the level of airgap, lower right – the division of the scalar and vector potential domains.

Vector \mathbf{A} and the scalar V_m domains are connected using a continuity condition implicitly implemented in COMSOL, Fig. 1 – bottom right, which ensures the continuity of the normal component of the magnetic flux density and the tangential component of the magnetic field strength. To compute the electromagnetic torque, T , *Arkkio's relation* was used [10], as it provides more accurate results than the default method implemented in COMSOL based on Maxwell's tensor [11]:

$$T = \frac{1}{\mu_0(r_i - r_e)} \int_{vol} r B_n B_t dv. \quad (4)$$

The relation integrates over the volume of the airgap comprised between the inner radius r_i and the outer radius r_e ; B_n and B_t are the normal and tangential components of the magnetic flux density, respectively. A more detailed analysis of combining vector and scalar magnetic potential in modelling the HSM was presented in [12].

The HSM model also contains the front ends of the stator windings and an air envelope surrounding the motor to

account for the magnetic leakage field and fringing. On the outer surfaces of the model, representing half of the HSM's cross-section and half of its axial length, a homogeneous Dirichlet condition was imposed, and on the lateral surfaces, a condition of periodicity of the magnetic field was imposed.

The active winding in the stator was modelled using COMSOL's *Coil* module with the *Numeric* option selected, which allows for the distribution of current density to be determined numerically based on the actual geometry of the coil. The coil type chosen was *Homogenized multiturn*, indicating the coil is constructed with multiple wires, with no eddy currents and skin effect. The number of turns and the phase current were imposed. Similar models of HSM were presented in [13] and [14], but without considering the end winding geometry and magnetic anisotropy.

2.1. MATERIALS USED. MODELING THE MAGNETIC ANISOTROPY

The stator and rotor of the HSM are constructed from a 50-50% iron-cobalt alloy, specifically *Vacoflux 50* in the stator [12] and *Vacodur* in the rotor. These materials have a high magnetic saturation knee, around 2.2 T, and are suitable for products designed for space applications, like the current HSM. The permanent magnets used are made of $\text{Sm}_2\text{Co}_{17}$, which have a remnant magnetic flux density B_r of 1.1 T and an equivalent relative magnetic permeability of 1.09. Although NdFeB magnets have a higher energy density, they are not approved for space applications due to their susceptibility to corrosion and a lower demagnetisation temperature than SmCo magnets.

Two models were developed: one with a solid stator made of *Vacoflux 50* and the other with a laminated stator. The first model has the stator and rotor made of homogeneous ferromagnetic materials, characterised by the same magnetisation characteristics for all three axes. The second model has a laminated stator made of thin insulated sheets bound together with adhesive. The insulation and adhesive form a thin layer of microns with a magnetic permeability equal to air permeability, significantly smaller than that of *Vacoflux 50*. As a result, the magnetic permeability is high along the surface of the laminations but much lower in the axial direction Oz .

Let us consider the magnetic reluctance corresponding to the iron part of a lamination \mathfrak{R}_{Fe} and that of the bilateral insulation of the lamination \mathfrak{R}_{in} :

$$\mathfrak{R}_{Fe} = \frac{\delta_{Fe}}{\mu_0 \mu_{r,Fe} S_{lam}}, \quad \mathfrak{R}_{in} = \frac{\delta_{in}}{\mu_0 S_{lam}}, \quad (5)$$

where δ_{Fe} is the thickness of the iron sheet, δ_{in} is the bilateral thickness of the sheet insulation, $\mu_{r,Fe}$ is the relative magnetic permeability of the ferromagnetic material, μ_0 the magnetic permeability of air, and S_{lam} is the section of the lamination. Based on the above relations it yields the expression of reluctance \mathfrak{R}_{stack} of the lamination stack made of N sheets [6]:

$$\begin{aligned} \mathfrak{R}_{stack} &= \frac{N \delta_{Fe}}{\mu_0 \mu_{r,Fe} S_{lam}} + \frac{N \delta_{in}}{\mu_0 S_{lam}} = \\ &= \frac{k_{Fe} l_{ax}}{\mu_0 \mu_{r,Fe} S_{lam}} + \frac{(1 - k_{Fe}) l_{ax}}{\mu_0 S_{lam}} = \frac{l_{ax}}{\mu_0 \mu_{r,Oz} S_{lam}} \end{aligned} \quad (6)$$

where l_{ax} is the stack length and $k_{Fe} = N \delta_{Fe} / l_{ax}$ is the stacking factor. From this, it follows the relative magnetic

permeability along the Oz direction $\mu_{r,Oz}$:

$$\frac{k_{Fe}}{\mu_{r,Fe}} + \frac{(1-k_{Fe})}{1} = \frac{1}{\mu_{Oz}} \Rightarrow$$

$$\Rightarrow \mu_{r,Oz} = \frac{\mu_{r,Fe}}{\mu_{r,Fe}(1-k_{Fe}) + k_{Fe}}$$
(7)

Since the ferromagnetic domain of the laminated stator is defined with the help of the magnetic vector potential \mathbf{A} , the magnetic flux density results as $\mathbf{B} = \text{rot } \mathbf{A}$. Hence, the material magnetic permeability of the homogenous material is $\mu = f(B)$, where $B_{Fe} = \sqrt{B_x^2 + B_y^2 + B_z^2}$, while the relative magnetic permeability is computed using eq. (2.7).

3. NUMERICAL RESULTS

The main design specifications of the HSM are, as follows: the number of phases $N_f = 2$ with redundant winding, 1° step, rated voltage $U_n = 26 \text{ V} \pm 10\%$, the phase resistance $R_{ph} \geq 55 \Omega \pm 5\%$; the phase inductivity $L_{ph} = 250 \text{ mH} \pm 30\%$; the angular speed $\Omega = 64^\circ/\text{s}$; the detent torque $T_d < 50 \text{ mNm}$; the holding torque $T_{max} = 1 \text{ Nm} \pm 5\%$; the outer diameter $D_{ext} = 69 \text{ mm}$; the inner diameter $D_{in} = 41 \text{ mm}$; axial lath length $l_{ax} = 18.6 \text{ mm}$ and the airgap $\delta > 0.1 \text{ mm}$.

Figure 1 illustrates the magnetic flux density distribution for two versions of the HSM. The top image displays the motor with a laminated stator, while the bottom shows the HSM with a solid stator. The difference in magnetic field distributions between the two cases is quite noticeable. In the HSM with a solid stator, the stator yoke is more saturated, leading to a more uniform distribution of magnetic flux density.

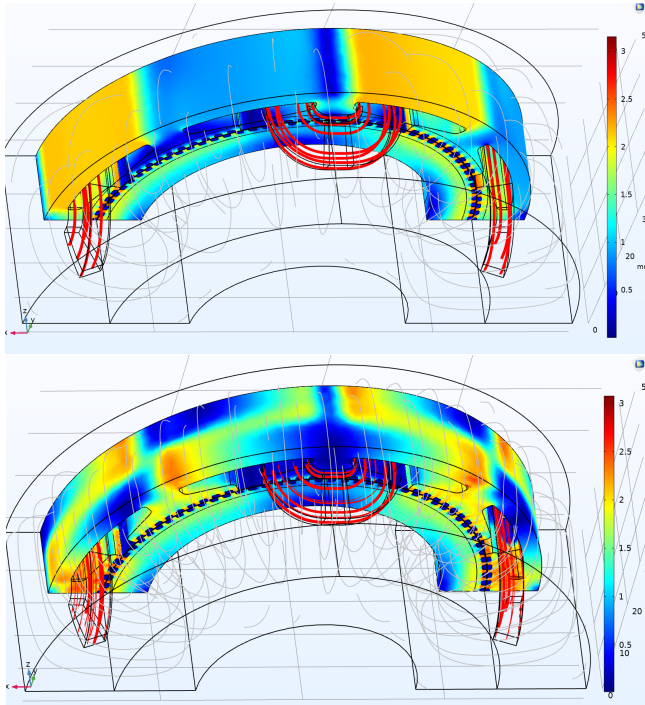


Fig. 2 – Magnetic flux density colour map, current density vectors, and magnetic leakage streamlines: top – HSM with stator made of laminations, bottom – HSM with the solid stator.

Another significant outcome is that the solution's convergence decreases due to the laminated stator's strong magnetic anisotropy. As a result, the computational time needed to resolve a solution for this model increases by at least three times compared to the computation of a similar

solution for the magnetically homogeneous model (the HSM with a solid stator).

3.1. COMPARISON BETWEEN THE HSM WITH A SOLID AND LAMINATED STATOR

The same geometry, materials, and supply voltage were used for modelling both HSMs: the one with a solid stator and the second having a laminated stator. Due to magnetic anisotropy with significantly reduced magnetic permeability along the axial direction, the HSM with a laminated stator produces a torque that is reduced by 20% at the rated current and about 18% at 0.8 A, compared to the HSM with a massive stator, as shown in figure 3.

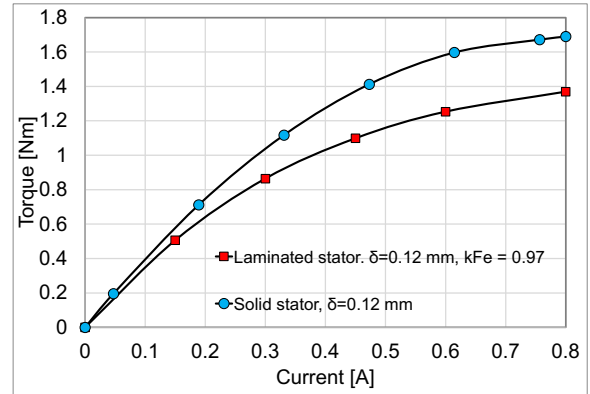


Fig. 3 – Holding torque versus current dependency for HSMs with a laminated and a solid stator, with airgap $\delta = 0.12 \text{ mm}$.

As shown in Fig. 2, the magnetic flux density colour map is different for the two HSMs, with a more constant distribution in the stator yoke along the axial direction for the HSM with a solid stator. A representation of the magnetic flux density along the Oz axis shows that significantly more magnetic flux closes through the shoe pole in the case of the HSM with a solid stator, Fig. 4.a) than in the case of the HSM with a laminated stator, Fig. 4.b).

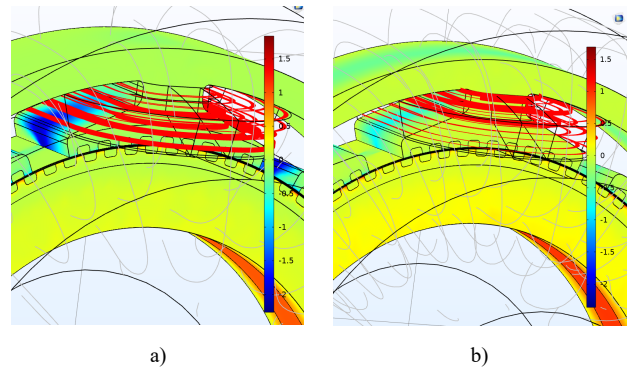


Fig. 4 – Magnetic flux density B_z , along Oz axis, at the level of the active pole for the two HSMs with: a) solid stator, b) laminated stator.

3.2. THE STACKING FACTOR AND AIRGAP INFLUENCE ON HSM TORQUE

In addition to the geometric parameters, two other factors influence the characteristics of the HSM: the stacking factor and the airgap dimension. According to relation (2.7), the magnetic relative permeability along the axial direction $\mu_{r,Oz}$ depends on the stacking factor k_{Fe} . For instance, reducing the stacking factor k_{Fe} from 0.98 to 0.97 decreases the average relative magnetic permeability from approximately 50 to 33.

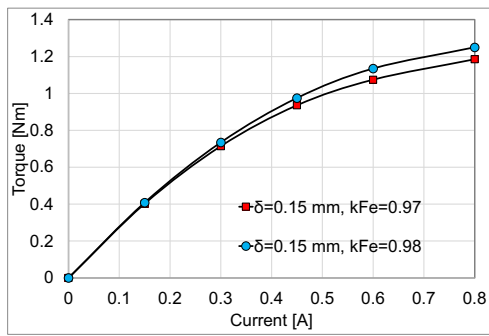


Fig. 5 – Holding torque versus current dependency for two stacking factors: $k_{Fe} = 0.98$ and $k_{Fe} = 0.97$ and airgap $\delta = 0.15$ mm.

This reduction subsequently leads to a decrease in the holding torque of the HSM, as illustrated in Fig. 5. However, if the airgap dimension remains unchanged (in this case, the airgap is $\delta = 0.15$ mm), the dependency between holding torque and current does not change much. Therefore, even without precise control over the stacking factor – which depends on the technology and materials used – numerical modelling can yield accurate results when designing an HSM.

A stronger impact on the HSM characteristic appears to be produced by the airgap modification. As shown in Fig. 6, increasing the airgap dimension from $\delta = 0.12$ mm to $\delta = 0.15$ mm produces an approximately 13% reduction of the holding torque at 0.8 A current. Notably, by increasing the airgap with only 0.01 mm at the same current, the torque decreased by 4%. This observation reinforces a well-known principle: the HSM torque density increases as the airgap decreases. This is why this motor is designed with minimal air gaps. [16].

The HSM static torque characteristic also depends on the airgap dimension. Figure 7 shows two static torque characteristics for two airgaps: $\delta = 0.12$ mm and $\delta = 0.15$.

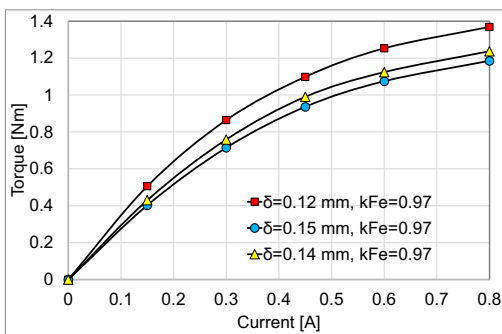


Fig. 6 – Holding torque versus current dependency for airgaps $\delta = 0.12$ mm, $\delta = 0.14$ mm, and $\delta = 0.15$ mm, and same stacking factor $k_{Fe} = 0.97$.

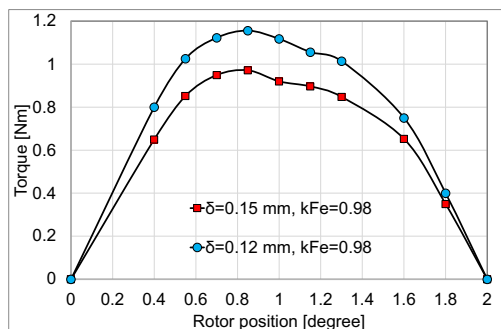


Fig. 7 – Static torque characteristics for airgaps $\delta = 0.12$ mm and $\delta = 0.15$ mm, and the same stacking factor $k_{Fe} = 0.98$.

4. MANUFACTURING THE HSM

A prototype HSM with laminated stator and redundant windings was manufactured for testing. Also, to verify manufacturing repeatability, two stators of Vacoflux 50, a cobalt-iron 0.35 mm lamination, and three solid rotors of Vacodur, were made, Figure 8. During this prototyping phase, the best stator-rotor combination was used to achieve the desired airgap. According to measurements, the airgap obtained value was about 0.13-0.14 mm.

The rotor has a "double stack" construction. The rotor crowns and the stator stack were cut using wire electric discharge machining. The middle rotor crown was twisted with 1° against the two side crowns and aligned with the help of three rivets, Fig. 9. Three notches were made on the permanent magnets rings made of Sm_2Co_{17} to allow indexing the rotor, Fig. 10.

A non-magnetic frame was designed for the stator, as the HSM has a frameless construction, Fig. 11. The rotor was placed on a non-magnetic shaft, Fig. 12, and centered within the stator, Fig. 12.



Fig. 8 – Two laminated stators and three solid rotors were manufactured.



Fig. 9 – Three rivets are used for rotor alignment.



Fig. 10 – The permanent magnet ring is made of Sm_2Co_{17} .

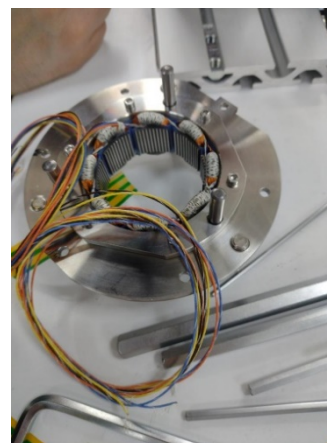


Fig. 11 – The stator is placed inside the frame.



Fig. 12 – The rotor is fixed on the shaft.

5. TEST RESULTS

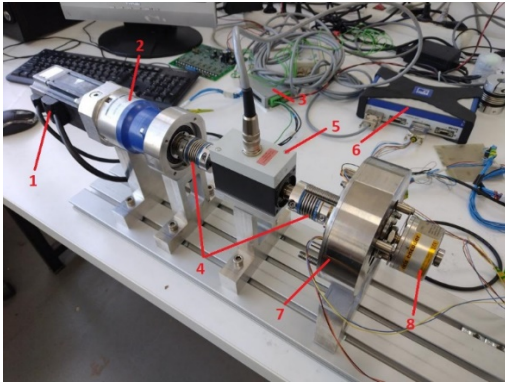


Fig. 13 – HSM testing bench.

Figure 13 shows the main components of the test bench: 1) servomotor with maximum torque 3.84 Nm and maximum speed 6000 rpm, 2) gearbox with ratio 1/100, 3) inverter, 4) elastic couplings, 5) 2 Nm torque transducer with accuracy of 0.04 Nm, 6) data acquisition system, 7) chassis-mounted HSM, and 8) encoder with 25000 lines/pulses.

The HSM torque has been measured at a very low and constant speed of 1/10 rpm to eliminate the influence of dynamic torque. To verify the repeatability of the measurement process, the static torque characteristic was measured five times for the same current applied in the stator. Each set of measurements was made for a full rotation of the HSM, by turning the rotor in the same direction.

Fig. 14 shows the HSM static torque curve obtained at 0.439 A, subtracting the friction torque produced by the measuring stand. The curve has a period of 4° as expected, and presents a slight subharmonic, most likely due to a slight shaft eccentricity.

Fig. 15 shows the static torque characteristics determined for different currents. The maximum static torque, i.e., the holding torque, is about 1 Nm and was obtained at a current of 0.439 A.

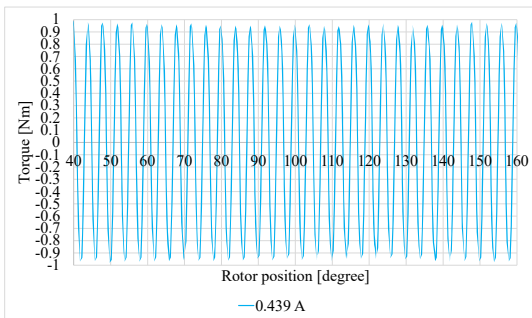


Fig. 14 – The HSM static torque characteristic.

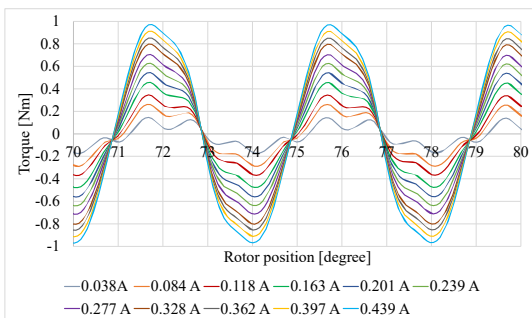


Fig. 15 – The HSM static torque characteristics obtained for different stator currents.

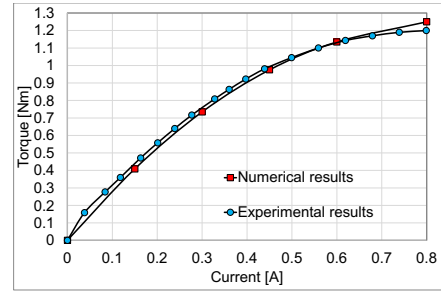


Fig. 16 – The holding torque vs current curve – numerically and experimentally determined.

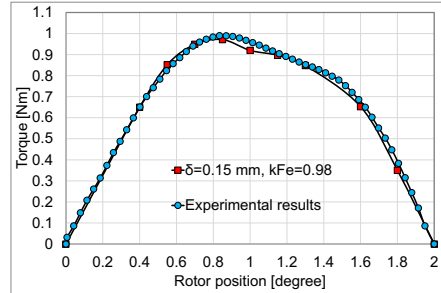


Fig. 17 – Comparison of the static torque characteristics, numerically and experimentally determined.

The holding torque versus current curve computed from the numerical model with a stacking factor k_{Fe} of 0.98 and an airgap δ of 0.15 mm, is very close to the experimentally determined curve (Figure 16). The same close results are seen in Figure 17 where the computed and experimentally determined curves of the HSM static torque are compared.

6. OPTIMIZING THE HSM WITH A LAMINATED STATOR

Following the calibration of the numerical model by considering the stacking factor in the stator $k_{Fe} = 0.98$ and the airgap $\delta = 0.15$ mm, for which the numerical results are very close to experimental measurements, the HSM was optimised to produce a higher holding torque. The geometric parameters used for optimisation include the stator poles' width, the stator yoke's height, the airgap diameter, and the coil's turns [9]. The conductor gauge was chosen so that the resistance of one phase is greater than 55Ω . The same design parameters that were described under § 3, were maintained.

The main geometrical differences between the optimised HSM and the initial, unoptimised HSM are an increased stator yoke and stator pole width, a higher airgap diameter, and the number of turns per coil decreased from 250 to 220. A detail of the two geometries is provided in Fig. 19.

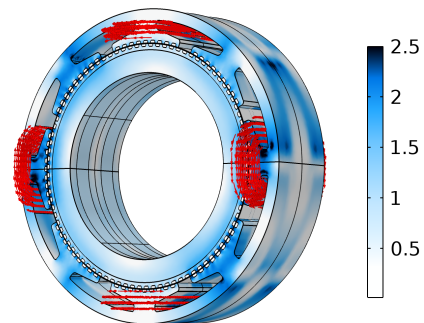


Fig. 18 – The magnetic flux density colour map and current density vectors (in red) in the entire HSM (recomposed from $1/4$ of the domain).

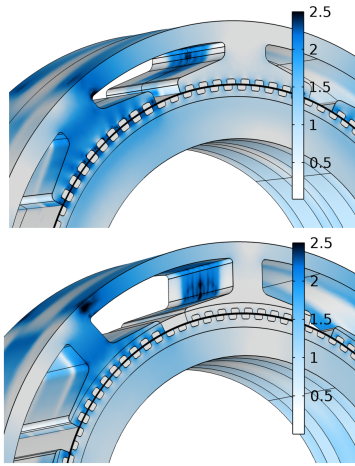


Fig. 19 – Optimized HSM (top) versus unoptimized HSM (bottom).

The optimization result shows an increase of 30 % of the holding torque at the rated current value of 0.47 A, Fig. 20, and a decrease of the electric time constant $T_e = L/R$ in the ratio of the square of the coil turns, $(220/250)^2 = 0.77$.

Figure 21 shows the two static torque characteristics of the optimised and initial HSM.

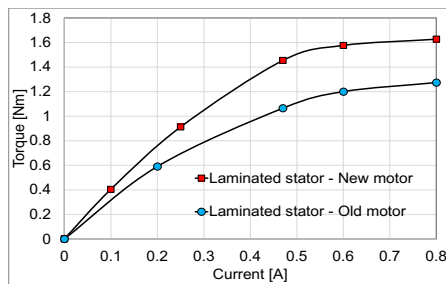


Fig. 20 – Holding torque versus current for the optimised and initial HSM.

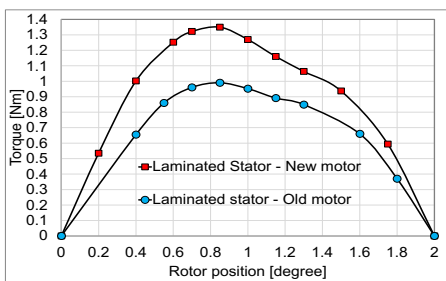


Fig. 21 – Static torque for the optimised and initial HSM.

7. CONCLUSIONS

The development of a 3D FEM numerical model with parameterized geometry enabled the analysis of the influence of geometric quantities on the HSM torque. It was found that slight deviations in the airgap, from 0.12 mm to 0.15 mm, produce a 15% decrease in holding torque, and a change in the stacking factor from 0.98 to 0.97 results in a reduction in holding torque of approximately 5%. However, these parameters depend on the manufacturing technology and achievable tolerances, making it difficult to calibrate the numerical model. Adjusting the airgap and stacking factor values in the numerical model was able to obtain differences between the numerical and experimental results of less than 5%. Using the 3D FEM model that considers the magnetic anisotropy produced by the stator laminations, the HSM has been optimized. This motor produces a holding torque of 1.37 Nm, greater than the 1 Nm produced by the measured

prototype. The concordance between the numerical results and the experimental measurements, as well as the significant increase in the HSM holding torque, shows the accuracy and effectiveness of the numerical modelling.

ACKNOWLEDGMENT

The authors would like to thank ICPE S.A. (www.icpe.ro), MESSICO department, for manufacturing the HSM prototype and allowing the authors to participate in its measurements.

CREDIT AUTHORSHIP CONTRIBUTION STATEMENT

Teodor Ionuț Ichim: Run the calculations in COMSOL, prepared the graphs, and participated in the experimental testing.
Ovidiu Craiu: Developed the FEM model and wrote the paper.

Received on 14 January 2025

REFERENCES

1. K.B. Jang, et al., *2-D FE analysis of hybrid stepping motor using virtual magnetic barrier*, IEEE Transactions on Magnetics, **39**, 5, pp. 3268–3270 (2003).
2. S.S.G. Kang, D.K. Lieu, *Torque analysis of combined 2D FEM and lumped parameter method for a hybrid stepping motor*, IEEE International Conference on Electric Machines and Drives, pp. 1199–1203 (2005).
3. C. Stuebig, B. Ponick, *Comparison of calculation methods for hybrid stepping motors*, IEEE Transactions on Industry Applications, **48**, 6, pp. 2182–2189 (2012).
4. K.R. Rajagopal, B. Singh, B.P. Singh, *Optimum tooth-geometry for hybrid stepper motor using finite element analysis*, 1998 International Conference on Power Electronic Drives and Energy Systems for Industrial Growth, Vol.1, pp. 264–269 (1998).
5. A. Oswald, H.G. Herzog, *Investigation of the usability of 2D- and 3D-FEM for a hybrid stepper motor*, 2009 IEEE International Electric Machines and Drives Conference, pp. 535–542 (2009).
6. S. Müller, M. Keller, A. Enssle, et al., *3D-FEM simulation of a transverse flux machine respecting nonlinear and anisotropic materials*.
7. C. Xia, H. Wang, Y. Wu, H. Wang, *Joining of the Laminated Electrical Steels in Motor Manufacturing: A Review*.
8. T.V. Jayaraman, *Effect of processing of HIPERCO 50 alloy laminates on their magnetic properties*, Journal of Electronic Materials, **44**, 11 (2015).
9. O. Craiu, T.I. Ichim, L.M. Melcescu, L. Popescu, *Optimization of a high torque density small hybrid stepper using 3D FEM model*, 2022 International Symposium on Power Electronics, Electrical Drives, Automation and Motion (SPEEDAM), pp. 610–615 (2022).
10. A. Arkkio, *Analysis of Induction Motors Based on the Numerical Solution of the Magnetic Field and Circuit Equations*, PhD Thesis (1987).
11. <https://doc.comsol.com/6.3/docs/server/#!/com.comsol.help.comsol/helpdesk/helpdesk.html>.
12. O. Craiu, T.I. Ichim, L.C. Popescu, *3D FEM Model of a Hybrid Stepper Using Scalar-Vector Potential Formulations*, 2023 13th International Symposium on Advanced Topics in Electrical Engineering (ATEE), pp. 1–5 (2023).
13. T.I. Ichim, O. Craiu, L.C. Popescu, *Analyzing a Three Hundred Teeth Bi-Phase Hybrid Stepper Motor with Different Numbers of Pole Pairs*, Rev. Roum. Sci. Techn. – Électrotechn. Et Énerg., **68**, 3, pp. 283–288 (2023).
14. I. Ionică, M. Modreanu, A. Morega, C. Boboc, *Numerical analysis of a hybrid stepper motor for the electromagnetic torque calculation*, 11th International Symposium on Advanced Topics in Electrical Engineering (ATEE) (2019).
15. <https://vacuumschmelze.com/products/soft-magnetic-materials-and-stamped-parts/lamination-stacks>.
16. M. Onsal, Y. Demir, M. Aydin, M.K. Guven, *Impact of Airgap on the Performance of 3-Phase Permanent Magnet Hybrid Stepper Motor*, IECON 47th Annual Conference of the IEEE Industrial Electronics Society, pp. 1–5 (2021).